

# Nanoscale

Accepted Manuscript



This is an *Accepted Manuscript*, which has been through the Royal Society of Chemistry peer review process and has been accepted for publication.

*Accepted Manuscripts* are published online shortly after acceptance, before technical editing, formatting and proof reading. Using this free service, authors can make their results available to the community, in citable form, before we publish the edited article. We will replace this *Accepted Manuscript* with the edited and formatted *Advance Article* as soon as it is available.

You can find more information about *Accepted Manuscripts* in the [Information for Authors](#).

Please note that technical editing may introduce minor changes to the text and/or graphics, which may alter content. The journal's standard [Terms & Conditions](#) and the [Ethical guidelines](#) still apply. In no event shall the Royal Society of Chemistry be held responsible for any errors or omissions in this *Accepted Manuscript* or any consequences arising from the use of any information it contains.

## ARTICLE

# Tuning the reorganization energy of electron transfer in supramolecular ensembles – metalloporphyrin, oligophenylenevinyls, and fullerene – and the impact on electron transfer kinetics

Cite this: DOI: 10.1039/x0xx00000x

Received 00th January 2012,  
Accepted 00th January 2012

DOI: 10.1039/x0xx00000x

www.rsc.org/

Christina Stangel<sup>1#</sup>, Christina Schubert<sup>3#</sup>, Susanne Kuhri<sup>3</sup>, Georgios Rotas<sup>2</sup>, Johannes T. Margraf<sup>3, 4</sup>, Elzbieta Regulska<sup>5</sup>, Timothy Clark<sup>4\*</sup>, Tomás Torres<sup>6, 7</sup>, Nikos Tagmatarchis<sup>2\*</sup>, Athanassios G. Coutsolelos<sup>1\*</sup>, Dirk M. Guldi<sup>3\*</sup>

Oligo(*p*-phenylenevinylene) (oPPVs) wires of various lengths featuring pyridyls at one terminal and C<sub>60</sub> moieties at the other, have been used as molecular building blocks in combination with porphyrins to construct a novel class of electron donor-acceptor architectures. These architectures, which are based on non-covalent, directional interactions between the zinc centers of the porphyrins and the pyridyls, have been characterized by nuclear magnetic resonance spectroscopy and mass spectrometry. Complementary physico-chemical assays focused on the interactions between the electron donors and acceptors in the ground and excited states. No appreciable electronic interactions were noted in the ground state, which was probed by electrochemistry, absorption spectroscopy, etc.; the electron acceptors are sufficiently decoupled from the electron donors. In the excited state, a different picture evolved. In particular, steady-state and time-resolved fluorescence and transient absorption measurements revealed substantial electron donor-acceptor interactions. These led upon photoexcitation of the porphyrins to tunable intramolecular electron-transfer processes, that is, the oxidation of the porphyrin and the reduction of C<sub>60</sub>. In this regard, the largest impact stems from a rather strong distance dependence of the total reorganization energy in stark contrast to the distance independence seen for covalently linked conjugates.

## Introduction

Natural processes of photosynthesis have increasingly inspired the fabrication of nanostructured molecular materials with advanced light-harvesting and electron-transfer features.<sup>1-6</sup> In this context, supramolecular chemistry allows diverse and disparate molecular building blocks to be amalgamated into highly ordered architectures. These mimic the key functions of the photosynthetic reaction center; light harvesting, charge separation, charge transport, and catalysis.<sup>7-10</sup> Porphyrinoids, the basic building block of chlorophylls, have emerged as an exceptional class of light harvesters and electron donors in such supramolecular electron donor-acceptor hybrids. This is mainly because porphyrinoids absorb a large fraction of the visible light (with extinction coefficients as high as 10<sup>5</sup> M<sup>-1</sup> cm<sup>-1</sup>) and because they give rise to remarkable redox chemistry.<sup>11, 12</sup> As a complement to porphyrinoids, fullerenes, in general, and C<sub>60</sub>, in particular, have unique physico-chemical properties that render them versatile electron acceptors in their ground state. Their three-dimensional structure, low reduction potentials, and small

reorganization energy in electron transfer processes<sup>13, 14</sup> are most notable in this context. Among others, these are important prerequisites for powering unidirectional electron-transfer processes and controlling the corresponding efficiencies and rates.<sup>15, 16</sup>

The conjugated nature of oPPVs also provides some structural rigidity between their termini. For example, only rotational motions about the formal single bonds are thermally accessible at room temperature. Thus, incorporation of rigid oPPVs into electron donor-acceptor architectures is an essential tool for fixing the spatial separation of electron donors and acceptors at the opposing termini. The oPPVs also play a mediating role in charge-separation and recombination processes without, however, actively participating in the electron transport at room temperature.<sup>17, 18</sup> Their electron donor and acceptor levels, on one hand, and those of the electron donors and acceptors, on the other, are decisive in favoring a coherent tunneling mechanism. For example, the electron acceptor levels of the oPPVs should

be higher than those of the light harvester/electron donor and of the electron acceptor.

In the context of oPPVs and  $C_{60}$ , molecular architectures that give rise to consecutive energy- and electron-transfer processes to  $C_{60}$  upon photoexcitation have been constructed using fullerene-based dendritic structures and oPPVs.<sup>19-24</sup> As a further elaboration, electron donors, such as ferrocene etc. have been attached covalently to  $C_{60}$ -oPPVs and the resulting conjugates probed by means of photophysical and electrochemical techniques.<sup>25</sup>

More recently, investigations have focused on advanced electron donor-acceptor conjugates. Most notably, oPPV conjugates carrying  $C_{60}$  as electron acceptor and either metalloporphyrins (ZnP) or  $\pi$ -extended tetrathiafulvalenes (exTTF) as electron donors have been designed and tested with particular focus on their physico-chemical properties.<sup>17, 18, 26, 27</sup> Long-lived charge-separated states were identified in  $C_{60}$ -oPPV-ZnPs as products of a rapid deactivation of the ZnP singlet excited state.<sup>28, 29</sup> In  $C_{60}$ -oPPV-ZnPs, the electron-transfer rates for the fast charge separation and slow charge recombination are near the top and inverted region of the Marcus parabola, respectively. A key factor for such a parabolic Marcus relationship is the total reorganization energy, which stems from both the electron donors and the electron acceptors.<sup>30, 31</sup> This is small in  $C_{60}$ -oPPV-ZnPs because of the formation of highly delocalized ZnP radical cations and  $C_{60}$  radical anions. Linking the oPPVs to the phenyls of ZnP also provides a beneficial contribution to keeping the total reorganization energy small.

A plethora of  $C_{60}$ -oPPV conjugates has been reported, including examples in which the length and the number of oPPVs were altered systematically in order to establish the relationship between electron-transfer rates and electron donor-acceptor distances.<sup>29, 32-37</sup> Attenuation factors as small as 0.01 Å<sup>-1</sup> were derived from the measured distance dependences of electron transfer for both charge separation and recombination processes. The reorganization energies for electron transfer in these  $C_{60}$ -oPPVs and, more importantly, their distance dependence has never been investigated in detail. Nevertheless, these studies gave no indication of a change in the outcome of the excited-state deactivation or in the associated kinetics.

Self-assembling discrete molecular building blocks in a specific and well-ordered way *en route* to architectures with precise functions such as photoinduced charge transfer phenomena,<sup>38-40</sup> constitutes an intriguing aspect of supramolecular chemistry.<sup>41, 42</sup> To the best of our knowledge, supramolecular assemblies of light-harvesting/electron-donating porphyrins and oPPVs of different lengths in the presence of electron accepting  $C_{60}$  have never been carried out. Thus, it is timely and necessary to assemble such architectures and to test their efficiencies in terms of charge-transfer events.

Our aim in this work is to approach a number of objectives systematically. Firstly, to functionalize  $C_{60}$  with a series of oPPVs of different lengths and carrying pyridyl moieties –  $C_{60}$ -oPPV-pyr. The pyridyls in  $C_{60}$ -oPPV-pyrs are essential as anchors to coordinate ZnP and to enable formation of novel

electron donor/acceptor architectures –  $C_{60}$ -oPPV-pyr•ZnP. Secondly, to characterize in detail the newly formed  $C_{60}$ -oPPV-pyr•ZnPs by, for example, nuclear magnetic resonance spectroscopy, mass spectrometry, electrochemistry, etc. Thirdly, to explore the basic electron-transfer phenomena in the novel electron donor acceptor  $C_{60}$ -oPPV-pyr•ZnPs by steady-state and time-resolved photophysical techniques. Finally, to determine whether the oPPV length plays a key role in the formation of charge-separated states.

## Experimental section

**General Methods.** Reagents and solvents were purchased as reagent grade and used without further purification. All solvents were dried by the appropriate techniques.<sup>43</sup> **ZnTPP**<sup>44</sup> was prepared according to previously reported procedure. Thin layer chromatography was performed on silica gel 60 F<sub>254</sub> plates. Chromatography was carried out on SiO<sub>2</sub> (silica gel 60, SDS, 70–230 mesh ASTM). HPLC separations were performed on a LC-9101 instrument using a CosmosilBuckyprep 20 x 250 mm preparative column and toluene as mobile phase at 10 mL min<sup>-1</sup>.

**4-[(bromotriphenylphosphoranyl)methyl]pyridine (2):** The salt **1** (0.500 mg, 1.98 mmol) and Na<sub>2</sub>CO<sub>3</sub> (0.21 g, 1.98 mmol) were dissolved in 2 mL of water and then the obtained solution was extracted with diethyl ether (50 mL) until all the desired 4-(bromomethyl) pyridine was obtained. To the combined extracts, toluene (20 mL) was added, and the mixture was distilled until all the diethyl ether was evaporated. Then triphenylphosphine (0.754 g, 2.88 mmol) was added and the mixture was heated at reflux for 3 h. The white precipitate was filtered, washed with toluene and subsequently dried under vacuum. This afforded the monophosphonium salt **2** as a white solid (0.380 g, 44.3 %). <sup>1</sup>H NMR (500 MHz, CDCl<sub>3</sub>): δ 8.30 (sb, 2H), 7.85 – 7.80 (m, 6H), 7.76 (m, 3H), 7.60–7.57 (m, 6H), 7.23 (sb, 2H), 5.80 (d, *J* = 16 Hz, 2H). <sup>13</sup>C NMR (125 MHz, CDCl<sub>3</sub>): 149.7, 138.1, 135.2, 134.5, 130.3, 126.9, 177.5, 29.7. HRMS (MALDI-TOF): *m/z* calcd for C<sub>24</sub>H<sub>21</sub>BrNP: 433.0595 [M]<sup>+</sup>. Found: 433.0601.

**4-{(E)-4-[(E)-2,5-bis(dodecyloxy)-4-((E)-2-(pyridin-4-yl)vinyl)styryl]-2,5-bis(dodecyloxy)styryl]-2,5-bis(dodecyloxy)benzaldehyde (E-5):** To a solution of **3** (0.20 g, 0.138 mmol) and **2** (0.060 g, 0.138 mmol) in dry methylene chloride (100 mL) lithium ethoxide solution (0.360 mL, 1.0 M in ethanol) was added dropwise at room temperature. The resulting solution was stirred for 20 min more after the completion of base addition. The reaction was quenched by the addition of dilute aqueous HCl. The organic layer was separated, washed with water, dried (Na<sub>2</sub>SO<sub>4</sub>), filtered and concentrated. In the resulting residue observed traces of the *Z* isomer, in a 97:3 ratio. Column chromatography (SiO<sub>2</sub>, CH<sub>2</sub>Cl<sub>2</sub>/EtOH, 100:0.5) gave **E-5** (0.13 g, 61.8%) as an orange fluorescent solid. <sup>1</sup>H NMR (300 MHz, CDCl<sub>3</sub>): δ 0.87–0.88 (m, 18H), 1.34 (m, 96H), 1.53 (m, 12H), 1.87 (m, 12H), 4.06 (m, 12H), 7.07 (AB, *J* = 16 Hz, 1H), 7.11 (s, 1H), 7.15 (s, 1H), 7.16 (s, 1H), 7.18 (s, 1H), 7.21 (s 1H), 7.33 (s, 1H), 7.44 (d, *J* = 5 Hz, 2H), 7.51 (m, 3H), 7.60 (AB, *J* = 16.5 Hz, 1H), 7.72 (AB, *J* = 16.5 Hz, 1H), 8.57 (sb, 2H), 10.45 (s, 1H). <sup>13</sup>C NMR (125 MHz, CDCl<sub>3</sub>): 189.3, 156.4, 151.9, 151.6, 151.3, 151.1, 150.8, 149.1, 146.6, 135.3, 129.4, 129.2, 128.2, 127.2, 126.1, 125.5, 125.2, 124.5, 124.2, 123.7, 123.0, 121.1, 111.3, 111.0, 110.7, 110.5, 110.3, 69.5, 32.0, 29.4, 26.4, 22.8, 14.2. HRMS (MALDI-TOF): *m/z* calcd for C<sub>102</sub>H<sub>167</sub>NO<sub>7</sub>: 1518.2743 [M]<sup>+</sup>. Found: 1518.2735.

**(E)-2,5-bis(dodecyloxy)-4-[2-(pyridin-4-yl)vinyl]benzaldehyde(E-6).** To a solution of **4** (0.19 g, 0.380 mmol) and **2** (0.166 g, 0.380 mmol) in dry methylene chloride (25 mL) lithium ethoxide solution (1 mL, 1.0 M in ethanol) was added dropwise at room temperature. The resulting solution was stirred for 20 min more after the completion of base addition. The reaction was quenched by the addition of dilute aqueous HCl. The organic layer was separated, washed with water, dried (Na<sub>2</sub>SO<sub>4</sub>), filtered and concentrated. Column chromatography (SiO<sub>2</sub>, CH<sub>2</sub>Cl<sub>2</sub>/EtOH, 100:0.1) gave **6** as an *E:Z* isomer mixture in a 90:10 ratio. A second column chromatography (SiO<sub>2</sub>, toluene/EtOAc, 100:5) gave **E-6** in pure form (0.144 g, 66%) as a yellow fluorescent solid. <sup>1</sup>H

NMR (500 MHz,  $\text{CDCl}_3$ ):  $\delta$  0.87 (m, 6H), 1.30 (m, 32H), 1.49 (m, 4H), 1.85 (m, 4H), 4.04 (t,  $J = 6.5$  Hz, 2H), 4.10 (t,  $J = 6.5$  Hz, 2H), 7.16 (s, 1H), 7.17 (AB,  $J = 16.5$  Hz, 1H), 7.34 (s, 1H), 7.39 (d,  $J = 6$  Hz, 2H), 7.65 (AB,  $J = 16.5$  Hz, 1H), 8.60 (d,  $J = 6$  Hz, 2H), 10.46 (s, 1H).  $^{13}\text{C}$  NMR (125 MHz,  $\text{CDCl}_3$ ):  $\delta$  189.3, 156.1, 150.3, 151.2, 144.7, 132.8, 129.5, 127.8, 125.3, 123.5, 121.2, 111.4, 110.4, 69.3, 32.0, 29.8, 29.7, 29.7, 29.7, 29.5, 29.5, 29.4, 29.3, 26.3, 26.2, 22.8, 14.2. HRMS (MALDI-TOF):  $m/z$  calcd for  $\text{C}_{38}\text{H}_{59}\text{NO}_3$ : 577.4495  $[\text{M}]^+$ . Found: 577.4502.

**$\text{C}_{60}$ -PPV3-pyr:** A mixture of *E*-5 (0.084 g, 0.055 mmol),  $\text{C}_{60}$  (0.040 g, 0.055 mmol) and sarcosine (0.049 g, 0.55 mmol) in toluene (40 mL) was refluxed for 4 h. After cooling, the reaction mixture was transferred onto the top of a silica gel column and eluted with toluene to collect unreacted  $\text{C}_{60}$  (10 mg, 25%). Then further elution with a mixture of toluene and ethylacetate (100:5) gave the impure product which was purified by preparative HPLC (retention time = 10 min) resulting  $\text{C}_{60}$ -PPV3-pyr (0.052 g, 41%) as a sticky brown-orange solid.  $^1\text{H}$  NMR (500 MHz,  $\text{CDCl}_3$ ):  $\delta$  0.88 (m, 18H), 1.25-1.54 (m, 108H), 1.78-1.87 (m, 12H), 2.84 (s, 3H), 3.77 (m, 1H), 4.06 (m, 11H), 4.32 (d,  $J = 9.5$  Hz, 1H), 4.98 (d,  $J = 9$  Hz, 1H), 5.56 (s, 1H), 7.05 (AB,  $J = 16.5$  Hz, 1H), 7.10-7.16 (m, 5H), 7.40 (sb, 2H), 7.50 (m, 4H), 7.60 (s, 1H), 7.69 (AB,  $J = 16.5$  Hz, 1H), 8.57 (sb, 2H).  $^{13}\text{C}$  NMR (75 MHz,  $\text{CDCl}_3$ ):  $\delta$  156.9, 155.3, 154.6, 154.0, 152.2, 151.8, 151.2, 151.0, 149.8, 147.4, 146.9, 146.2, 146.1, 145.9, 145.7, 145.4, 145.3, 144.7, 144.5, 143.2, 142.8, 142.7, 142.3, 142.1, 141.9, 140.3, 139.9, 139.6, 136.6, 136.4, 136.3, 134.7, 129.4, 128.7, 127.8, 127.7, 127.3, 125.6, 125.1, 124.5, 124.0, 123.7, 123.2, 121.0, 115.0, 111.3, 110.8, 110.7, 110.5, 109.6, 75.9, 69.1, 69.7, 69.6, 68.7, 40.3, 32.07, 31.4, 29.7, 26.4, 22.8, 14.3. IR:  $\tilde{\nu}$  2919.77, 2849.80, 1591.55, 1462.94, 1420.50, 1030.55, 967.12, 850.59, 719.90, 526.47  $\text{cm}^{-1}$ . HRMS (MALDI-TOF):  $m/z$  calcd for  $\text{C}_{164}\text{H}_{173}\text{N}_2\text{O}_6$ : 2266.3294  $[\text{M} + \text{H}]^+$ . Found: 2266.3288.

**$\text{C}_{60}$ -PPV1-pyr:** A mixture of *E*-6 (0.044 g, 0.076 mmol),  $\text{C}_{60}$  (0.055 g, 0.076 mmol) and sarcosine (0.068 g, 0.76 mmol) in toluene (40 mL) was refluxed for 3 h. After cooling, the reaction mixture was transferred onto the top of a silica gel column and eluted with toluene to collect unreacted  $\text{C}_{60}$  (12.4 mg, 22.6%). Then further elution with a mixture of toluene and ethylacetate (100:5) gave the impure product which was purified by preparative HPLC (retention time = 17 min) resulting  $\text{C}_{60}$ -PPV1-pyr (0.043 g, 42.3%) as a sticky brown-orange solid.  $^1\text{H}$  NMR (300 MHz,  $\text{CDCl}_3$ ):  $\delta$  0.87 (m, 6H), 1.25 (m, 32H), 1.62-1.69 (m, 4H), 1.80 (m, 4H), 2.83 (s, 3H), 3.75 (m, 1H), 4.04 (m, 2H), 4.15 (m, 1H), 4.32 (d,  $J = 9.6$  Hz, 1H), 4.98 (d,  $J = 9.3$  Hz, 1H), 5.56 (s, 1H), 7.05 (AB,  $J = 16.5$  Hz, 1H), 7.10 (s, 1H), 7.36 (m, 2H), 7.60 (s, 1H), 7.66 (AB,  $J = 16.5$  Hz, 1H), 8.56 (sb, 2H).  $^{13}\text{C}$  NMR (75 MHz,  $\text{CDCl}_3$ ):  $\delta$  156.8, 155.1, 154.3, 152.1, 151.6, 149.8, 147.5, 147.4, 146.9, 146.8, 146.4, 146.3, 146.2, 146.1, 145.9, 145.8, 145.7, 145.6, 145.5, 145.4, 145.3, 144.7, 144.6, 144.5, 143.2, 142.8, 142.7, 143.2, 143.1, 142.8, 142.7, 142.5, 142.4, 142.3, 142.2, 142.1, 141.9, 141.9, 140.3, 139.8, 139.6, 136.4, 136.2, 134.8, 128.7, 127.6, 126.4, 125.7, 121.0, 115.0, 110.2, 70.0, 69.9, 69.4, 68.9, 40.3, 32.0, 29.6, 29.5, 29.4, 29.8, 14.3. IR:  $\tilde{\nu}$  2916.40, 2847.64, 1590.48, 1461.17, 1461.17, 1413.32, 1258.07, 1010.84, 792.55, 524.73  $\text{cm}^{-1}$ . HRMS (MALDI-TOF):  $m/z$  calcd for  $\text{C}_{100}\text{H}_{64}\text{N}_2\text{O}_2$ : 1324.4968  $[\text{M}]^+$ . Found: 1324.4979.

**NMR spectroscopy.**  $^1\text{H}$  NMR and  $^{13}\text{C}$  NMR spectra were recorded on Bruker AMX-500 MHz and Bruker DPX-300 MHz spectrometers as solutions in deuterated solvents by using the solvent peak as the internal standard.

**Mass spectrometry.** High-resolution mass spectra were performed on a Bruker ultrafleXtreme MALDI-TOF/TOF spectrometer using trans-2-[3-(4-tert-butylphenyl)-2-methyl-2-propenylidene] malononitrile as matrix.

**FTIR spectroscopy.** (ATR)-FTIR spectra were recorded on a Thermo-Electron Nicolet 6700 FTIR optical spectrometer with a DTGS KBr detector at a resolution of 4  $\text{cm}^{-1}$ .

**Electrochemistry.** Electrochemical data were obtained by cyclic voltammetry using a conventional single-compartment three-electrode cell arrangement in combination with a potentiostat "AUTOLAB®, eco chemie". As auxiliary and reference electrode Pt and Ag wires were used, while the

working electrode was a glassy carbon electrode. Tetrabutylammonium hexafluorophosphate ( $\text{TBAPF}_6 = 0.05$  M) was used as supporting electrolyte at room temperature. All potentials are referenced to ferrocene/ferrocenium.

**UV/vis absorption spectroscopy.** Steady state absorption spectra were obtained using a Perkin Elmer Lambda 2 UV/vis two-beam spectrophotometer with a slit width of 2 nm and a scan rate of 480 nm/min. A quartz glass cuvette of 10x10 mm was used.

**Emission spectroscopy.** Steady state emission was recorded using a Horiba Jobin Yvon FluoroMax-3 spectrometer using a slit width of 2 nm for excitation and emission and an integration time of 0.2 s. A quartz glass cuvette of 10x10 mm was used. All spectra were corrected for the instrument response. For excitation wavelength below 450 nm a cut off filter (435 nm) was inserted.

**Fs-transient absorption spectroscopy.** Femtosecond transient absorption studies were performed with laser pulses (1 kHz, 150 fs pulse width) from an amplified Ti/sapphire laser system (Model CPA 2101, Clark-MXR Inc.; output 775 nm). For an excitation wavelength of 420 and 550 nm, a nonlinear optical parametric converter (NOPA) was used to generate ultra-short tunable visible pulses out of the pump pulses. The transient absorption pump probe spectrometer (TAPPS) is referred to as a two-beam setup, in which the pump pulse is used as excitation source for transient species and the delay of the probe pulse is exactly controlled by an optical delay rail. As the probe (white-light continuum), a small fraction of pulses stemming from the CPA laser system was focused by a 50 mm lens into a 2 mm thick sapphire disc. The transient spectra were recorded using fresh argon-saturated solutions in each laser excitation. All experiments were performed at 298 K in a 2 mm quartz cuvette.

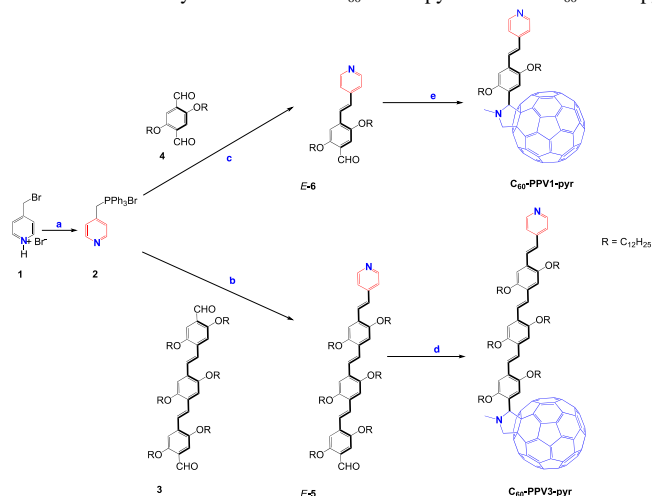
**Molecular Modeling.** Geometries and local properties were calculated using the semi-empirical AM1 Hamiltonian as implemented in EMPIRE<sup>12</sup>.<sup>45-47</sup> The local electron affinity<sup>48, 49</sup> was calculated from the resulting molecular orbitals.

## Results and discussion

**Synthesis.** The strategy employed for synthesizing  $\text{C}_{60}$  functionalized with oPPVs is based on the 1,3-dipolar cycloaddition of azomethine ylides, generated *in situ* upon thermal condensation of custom-synthesized oPPV-based aldehydes and sarcosine, to  $\text{C}_{60}$ .<sup>50</sup> The synthetic approach to the oPPV-based aldehydes relies on Wittig-type reactions.<sup>51</sup> Scheme 1 illustrates the synthesis of the two oPPV-based aldehydes of different lengths *E*-5 and *E*-6, both terminated with a pyridyl group, and the preparation of the corresponding  $\text{C}_{60}$ -PPV3-pyr and  $\text{C}_{60}$ -PPV1-pyr. Briefly, 2,5-bis(dodecyloxy)benzene-1,4-dialdehyde **4** was prepared in three steps from hydroquinone in 45% yield according to a modified method (see Supporting Information for details).<sup>52, 53</sup> Bis-aldehyde **3** was prepared in 81% yield from hydroquinone in five steps using a Wittig-reaction and also was prepared in seven steps using the Horner-Wadsworth-Emmons (HWE) reaction (see Supporting Information for details). Then, Wittig reaction of **3** in the presence of LiOEt with the pyridylphosphonium salt **2**, which was made from **1**, afforded the *E*-isomer of oPPV-based aldehyde *E*-5, along with traces (3%) of the *Z*-isomer. Column chromatography gave *E*-isomer **5** in pure form in 62% yield. Under a similar Wittig reaction, **4** gave access to the *E*-isomer of oPPV-based aldehyde *E*-6 (66% yield). Thus, with oPPV-based aldehydes *E*-5 and *E*-6 in hand,  $\text{C}_{60}$ -PPV3-pyr and  $\text{C}_{60}$ -PPV1-pyr were obtained on 1,3-dipolar cycloaddition in the presence of sarcosine. At this stage, it should be noted that  $\text{C}_{60}$ -PPV1-pyr and  $\text{C}_{60}$ -PPV3-pyr were purified by recycling HPLC (Buckyprep Cosmol column, 250 mm x 20 mm, toluene eluent, 10 mL  $\text{min}^{-1}$  flow rate) in 42% and 41%, respectively. The dodecyloxy groups as side chains of the  $\text{C}_{60}$ -PPV1-pyr and  $\text{C}_{60}$ -

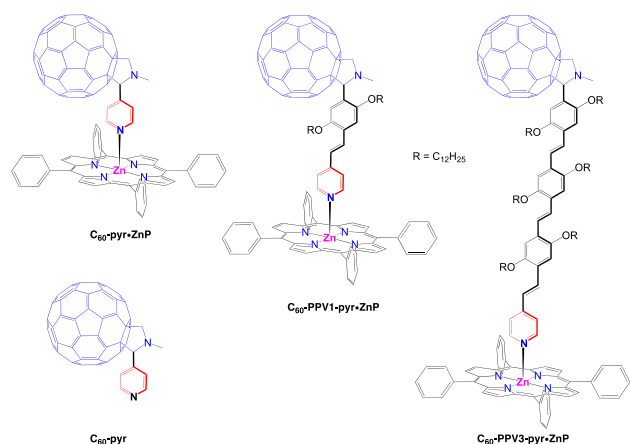
**PPV3-pyr**, provide enhanced solubility in common organic solvents such as toluene, dichloromethane, THF, etc. and thus for a complete spectroscopic characterization.

**Scheme 1.** Synthesis of  $C_{60}$ -PPV1-pyr and  $C_{60}$ -PPV3-pyr<sup>a</sup>



<sup>a</sup>Reagents and conditions: a) (i)  $\text{Na}_2\text{CO}_3$  (aq.)/ $\text{Et}_2\text{O}$ , (ii)  $\text{PPh}_3$ , toluene, reflux, 3h, 44%; b) **3**,  $\text{LiOEt}$ ,  $\text{CH}_2\text{Cl}_2$ , room temperature, 20 min, 62 %; c) **4**,  $\text{LiOEt}$ ,  $\text{CH}_2\text{Cl}_2$ , room temperature, 20 min, 66%; d) **E-5**,  $C_{60}$ , sarcosine, toluene, reflux, 4h, 41%; e) **E-6**,  $C_{60}$ , sarcosine, toluene, reflux, 3h, 42%.

**Scheme 2.** Hybrids  $C_{60}$ -pyr•ZnP,  $C_{60}$ -PPV1-pyr•ZnP,  $C_{60}$ -PPV3-pyr•ZnP and reference  $C_{60}$ -pyr



In brief, the characteristic  $^1\text{H}$  NMR pattern for the *E*-configuration of the vinylic protons in oPPVs includes a rather large coupling constant (16.5 Hz) for the corresponding AB system in  $C_{60}$ -PPV1-pyr and  $C_{60}$ -PPV3-pyr. Furthermore, their structures were confirmed by identifying their molecular ion peaks in the MALDI-TOF mass spectra;  $[\text{M}^+]$  1324.4979 for  $C_{60}$ -PPV1-pyr and  $[\text{M}^+]$  2266.3288 for  $C_{60}$ -PPV3-pyr.

**Electrochemical characterization.** The one-electron oxidations and reductions of  $C_{60}$ -pyr•ZnP,  $C_{60}$ -PPV1-pyr•ZnP, and  $C_{60}$ -PPV3-pyr•ZnP and their ZnP and  $C_{60}$ -PPV references were probed by cyclic voltammetry at room temperature in chlorobenzene (Table 1). For the references, the first reversible oxidation of ZnP appears at 0.33 V whereas the first and second reversible reductions of  $C_{60}$ -pyr,  $C_{60}$ -PPV1-pyr and  $C_{60}$ -PPV3-pyr appear at -1.24/-1.63, -1.24/-1.65 and -1.24/-1.65 V (vs.  $\text{Fc}^+/\text{Fc}$ ), respectively. In  $C_{60}$ -pyr•ZnP, the oxidation of ZnP is shifted to 0.31 V (vs.  $\text{Fc}^+/\text{Fc}$ ) and the first reduction of  $C_{60}$  occurs at -1.21 V (vs.  $\text{Fc}^+/\text{Fc}$ ). For  $C_{60}$ -PPV1-pyr•ZnP, and  $C_{60}$ -PPV3-pyr•ZnP, the ZnP oxidation and the  $C_{60}$  reduction are seen at 0.32 and -1.25 V (vs.  $\text{Fc}^+/\text{Fc}$ ), respectively, for both systems. Overall, the shifts are small with 10 mV. Nevertheless, all electron donor-acceptor ensembles show slightly easier oxidation as well as slightly easier reduction compared to their references. On careful examination of all of

the redox data, we conclude that the redox potentials in  $C_{60}$ -oPPV•ZnPs are subject to minor shifts due to the axial coordination when compared to the corresponding references.

**Table 1:** Electrochemical data

Compound	$E_{\text{ox}}^1$	$E_{\text{red}}^1$	$E_{\text{red}}^2$
ZnTPP	0.33		
$C_{60}$ -pyr		-1.24	-1.63
$C_{60}$ -PPV1		-1.24	-1.65
$C_{60}$ -PPV3		-1.24	-1.65
$C_{60}$ -pyr•ZnP	0.31	-1.21	
$C_{60}$ -PPV1•ZnP	0.32	-1.25	
$C_{60}$ -PPV3•ZnP	0.32	-1.25	

Potentials in V (half-wave potentials:  $E_{1/2}$ ); scan rate 100  $\text{mVs}^{-1}$ . Measurements were performed in chlorobenzene containing 0.1 M TBAPF<sub>6</sub> as supporting electrolyte with a glassy carbon working electrode, a platinum counter electrode, and a silver pseudo-reference electrode. Corrected for ferrocene as an internal standard.

**Steady-state photophysical characterization.** In the absorption spectra of  $C_{60}$ -PPV1-pyr and  $C_{60}$ -PPV3-pyr, the characteristic absorptions of the individual  $C_{60}$  and oPPV constituents are discernable (Figure 1). In particular,  $C_{60}$  absorbs between 250 and 300 nm, whereas the oPPVs exhibit broad maxima between 400 and 500 nm in  $C_{60}$ -PPV1-pyr and  $C_{60}$ -PPV3-pyr, respectively. It is important that the overall absorption characteristics depend on the length of the oPPVs; the red shift from 432 to 440 nm of the oPPV centered absorption in  $C_{60}$ -PPV1-pyr and  $C_{60}$ -PPV3-pyr as the overall oPPV length increases is consistent with extended  $\pi$ -conjugation. Please note that the absorption of  $C_{60}$ -pyr, which is used to complement the series, is identical to that of functionalized  $C_{60}$ .

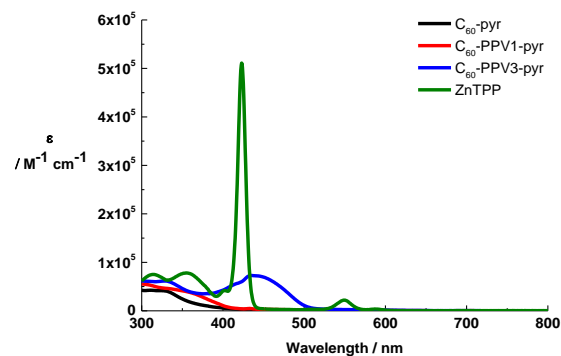


**Fig. 1.** Room temperature absorption spectra of ZnTPP (green),  $C_{60}$ -pyr (black)  $C_{60}$ -PPV1-pyr (red),  $C_{60}$ -PPV3-pyr (blue) in chlorobenzene.

Turning to fluorescence spectroscopy, the oPPV and  $C_{60}$  constituents emit singlet excited state energy in different spectral regions of the spectrum. Upon excitation at 420 nm, fluorescence of oPPV is evident at 514 nm for  $C_{60}$ -PPV3-pyr. Photoexcitation at 350 nm results, in stark contrast, in a weak emission due to  $C_{60}$  at 710 nm.<sup>50</sup>

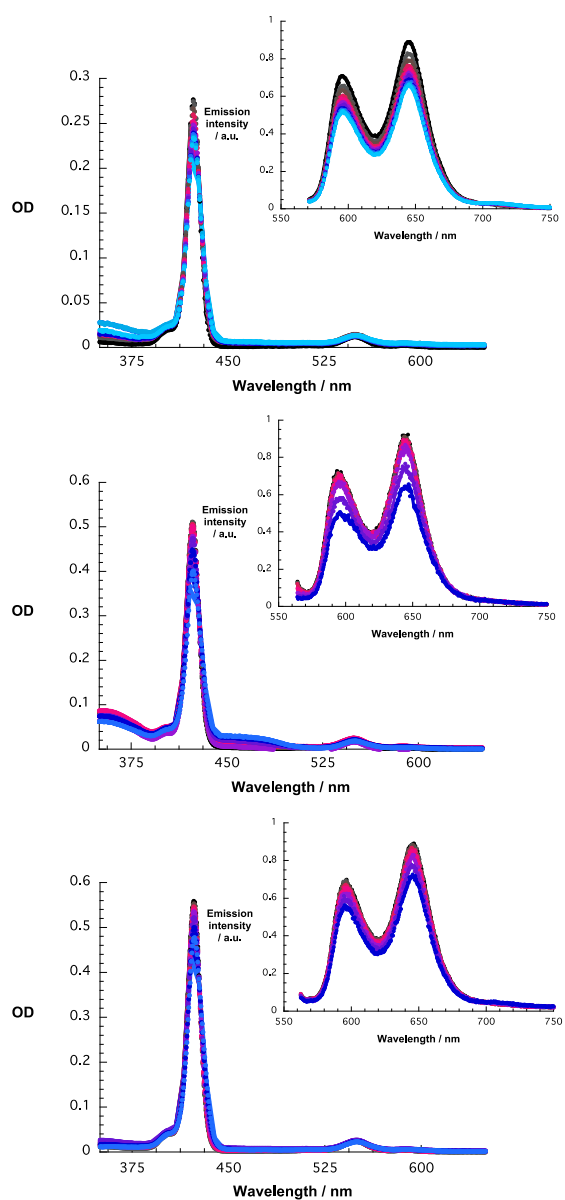


**Fig. 2.** Absorption spectra in chlorobenzene of ZnTPP ( $1.0 \times 10^{-6}$  M) with variable concentrations of upper part:  $C_{60}$ -PPV1-pyr ( $0 - 2.5 \times 10^{-5}$  M); middle part:  $C_{60}$ -PPV3-pyr ( $0 - 2.7 \times 10^{-5}$  M) and lower part:  $C_{60}$ -pyr ( $0 - 2.7 \times 10^{-5}$  M). Insert: corresponding fluorescence spectra of each titration excited at 556 nm.

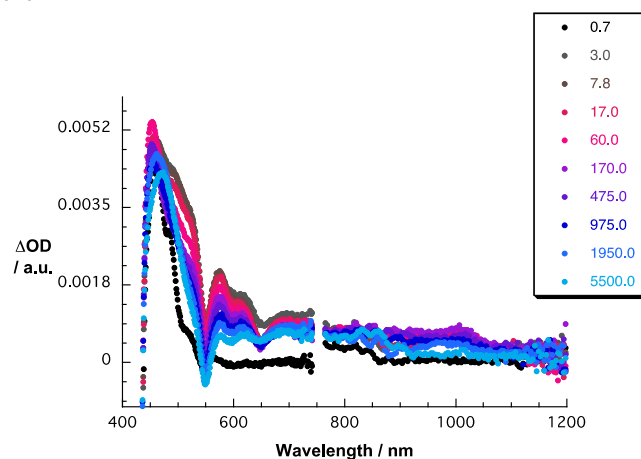
In an attempt to coordinate zinc tetraphenylporphyrin (ZnP) to  $C_{60}$ -pyr,  $C_{60}$ -PPV1-pyr, and  $C_{60}$ -PPV3-pyr several titration assays with focus on the ground and the excited states were performed. In the ground state, the interactions of  $C_{60}$ -pyr,  $C_{60}$ -PPV1-pyr, and  $C_{60}$ -PPV3-pyr with ZnP were followed by absorption spectroscopy in chlorobenzene. Absorption titrations were performed with, for example,  $10^{-6}$  M solutions of ZnP in the absence and presence of various concentrations of  $C_{60}$ -pyr,  $C_{60}$ -PPV1-pyr, and  $C_{60}$ -PPV3-pyr. The concentrations of the latter were increased incrementally from 0 to  $2.5 \times 10^{-5}$  M and substantial changes were discernable in the absorption spectra. In particular, the original Soret band at 423 nm decreases in intensity. This decrease is accompanied by the formation of a new Soret band at 430 nm that implies the coordination of ZnP to  $C_{60}$ -pyr,  $C_{60}$ -PPV1-pyr, and  $C_{60}$ -PPV3-pyr. Our hypothesis is corroborated by the development of an isosbestic point at 428 nm. Binding constants of  $1.2 \times 10^4$ ,  $0.7 \times 10^4$ , and  $2.5 \times 10^4$   $M^{-1}$  were derived from the underlying concentration vs absorption change relationships for  $C_{60}$ -pyr,  $C_{60}$ -PPV1-pyr, and

$C_{60}$ -PPV3-pyr, respectively. In addition, Job's plot analyses were carried out. Here, the aforementioned spectral changes associated with  $C_{60}$ -pyr•ZnP,  $C_{60}$ -PPV1-pyr•ZnP, and  $C_{60}$ -PPV3-pyr•ZnP at the Soret band maximum were used and plotted versus the mole fraction (Figure S1). Importantly, maxima are observed in all cases at mole fractions of 0.5, which suggest 1:1 stoichiometries for  $C_{60}$ -pyr•ZnP,  $C_{60}$ -PPV1-pyr•ZnP, and  $C_{60}$ -PPV3-pyr•ZnP. Insights into excited-state interactions came from steady-state fluorescence measurements of ZnP in chlorobenzene solutions that were excited at either 420 nm or 556 nm to match the absorption of the ZnP Soret band or Q band, respectively (Figure 2). In particular, the intensity of the ZnP-centered fluorescence, with maxima at 600 and 650 nm and quantum yields of 0.04, was found to depend on the concentrations of  $C_{60}$ -pyr,  $C_{60}$ -PPV1-pyr, and  $C_{60}$ -PPV3-pyr, indicating the gradual transformation of ZnP into  $C_{60}$ -pyr•ZnP,  $C_{60}$ -PPV1-pyr•ZnP, and  $C_{60}$ -PPV3-pyr•ZnP. Binding constants of  $0.94 \times 10^4$ ,  $1.8 \times 10^4$ , and  $2.0 \times 10^4$   $M^{-1}$  were obtained as  $\log K_{\text{ass}} = (x.x)$  by nonlinear-least-square curve fitting of the ZnP fluorescence quenching at 595 and 645 nm, for  $C_{60}$ -pyr,  $C_{60}$ -PPV1-pyr, and  $C_{60}$ -PPV3-pyr, respectively. Please note that these values are in excellent agreement with those derived from the absorption assays – *vide supra*.

**Time-resolved photophysical characterization.** The fluorescence titrations suggested a deactivation of the photoexcited electron donor-acceptor ensembles –  $C_{60}$ -pyr•ZnP,  $C_{60}$ -PPV1-pyr•ZnP, and  $C_{60}$ -PPV3-pyr•ZnP – via either an intramolecular energy or electron transfer between photoexcited ZnP and ground state  $C_{60}$ . To shed light onto the nature of the energy and/or electron transfer deactivation and the corresponding dynamics, we turned to femtosecond transient absorption experiments.

Representative differential absorption spectra taken, for example, upon 420 nm excitation of ZnP in chlorobenzene solutions, are shown in Figure S2. Here, the differential absorption spectra recorded immediately after the laser pulse are characterized by bleaching of the ZnP Q band at 560 nm and appearance of transients at 480 nm and between 580 and 750 nm. These are spectral attributes of the ZnP singlet excited state (2.04 eV). The latter decays slowly ( $4.0 \times 10^8$   $s^{-1}$ ) in anisole to the energetically lower-lying ZnP triplet excited state (1.53 eV) via intersystem crossing.

Now, considering the differential absorption spectra of  $C_{60}$ -pyr•ZnP,  $C_{60}$ -PPV1-pyr•ZnP, and  $C_{60}$ -PPV3-pyr•ZnP we probed different ratios of ZnP, on one hand, and  $C_{60}$ -pyr,  $C_{60}$ -PPV1-pyr, and  $C_{60}$ -PPV3-pyr, on the other. Specifically, ratios of 1:2, 1:5 and 1:10 ( $c(\text{ZnP}) = 5 \times 10^{-5}$  M) were used. To ensure selective excitation of ZnP, excitations at 420 and 550 nm were selected for  $C_{60}$ -pyr•ZnP,  $C_{60}$ -PPV1-pyr•ZnP, and  $C_{60}$ -PPV3-pyr•ZnP. The observation of an instantaneous growth of a broad absorption between 570 and 750 nm confirms the selective excitation of the ZnP in  $C_{60}$ -pyr•ZnP,  $C_{60}$ -PPV1-pyr•ZnP, and  $C_{60}$ -PPV3-pyr•ZnP (Figures 3-5). However, within the first few picoseconds, these excited-state features give place to a transient absorption in the near infrared region that maximizes at 1020 nm.



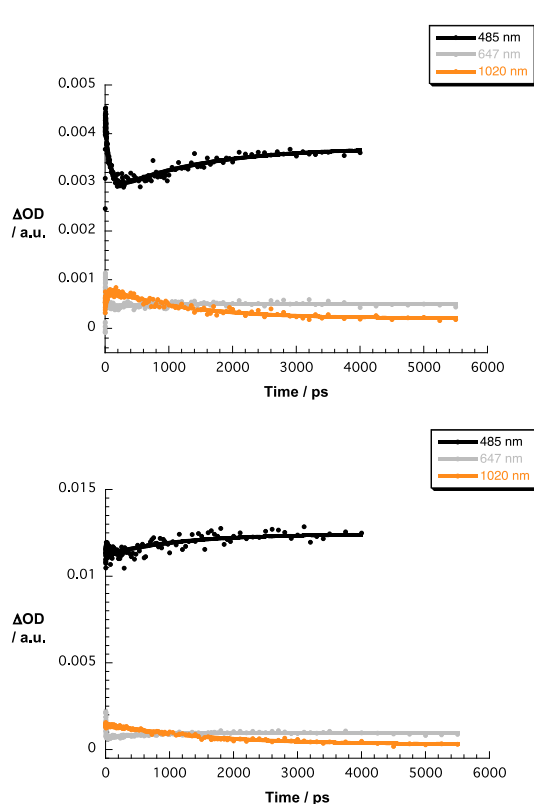


**Fig. 3.** Upper part – differential absorption spectra (visible and near-infrared) obtained upon pump probe excitation (420 nm, 200 nJ) of  $C_{60}$ -PPV1-pyr-ZnP (in a 1 to 5 ratio) in chlorobenzene with several time delays between -0.3 and 5500 ps at room temperature – see legend for details. Central part – time-absorption profiles of the spectra shown above at 485, 647, and 1020 nm monitoring the charge separation and charge recombination. Lower part – time-absorption profiles of the spectra in anisole at 485, 647, and 1020 nm monitoring the charge separation and charge recombination.

We infer the formation of the one-electron reduced  $C_{60}$  radical anion from these results.<sup>54</sup> In the visible, the absorption of the one-electron oxidized ZnP radical cation emerges in the region 600–700 nm. The latter is, however, to some extent masked by the much stronger ZnP triplet excited state as well as  $C_{60}$  triplet excited state features.<sup>55, 56</sup> Careful analyses of the absorption time profiles in the 600–700 nm and 900–1100 nm region enables the analysis of the charge-transfer rates of the ZnP radical cation and  $C_{60}$  radical anion, respectively. The charge separation lifetimes in anisole are 25 ps for  $C_{60}$ -pyr-ZnP, 2 ps for  $C_{60}$ -PPV1-pyr-ZnP, and 23 ps for  $C_{60}$ -PPV3-pyr-ZnP.

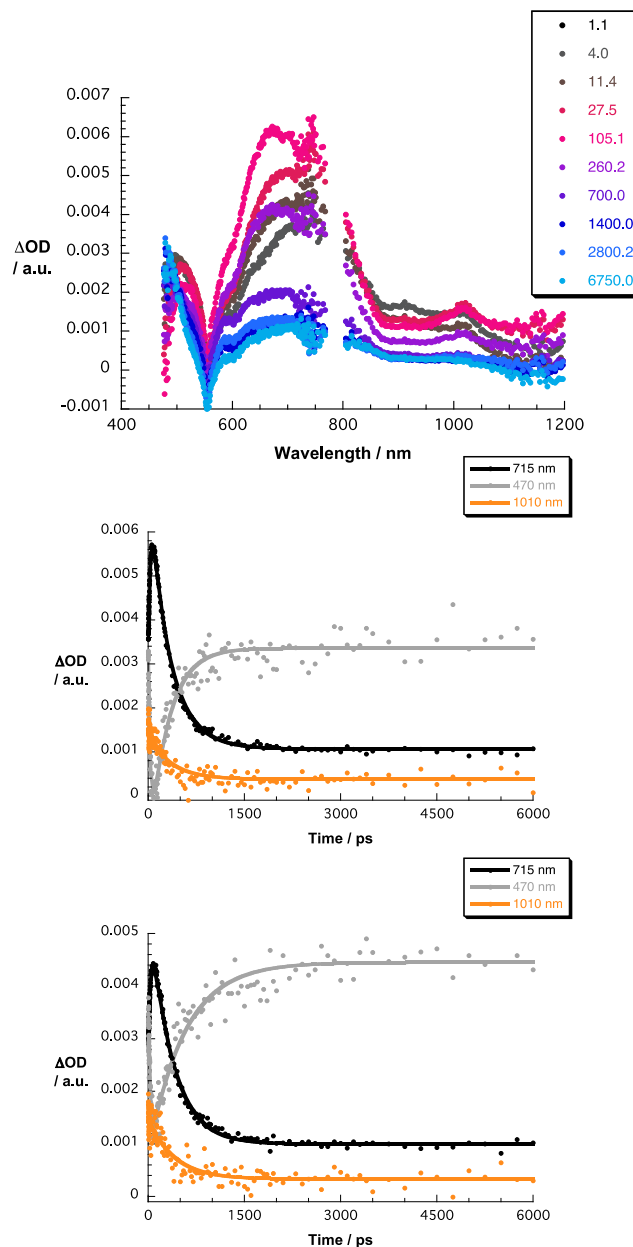


**Fig. 4.** Upper part – differential absorption spectra (visible and near-infrared) obtained upon pump probe excitation (550 nm, 200 nJ) of  $C_{60}$ -PPV3-pyr-ZnP (in a 1 to 5 ratio) in chlorobenzene with several time delays between 1.1 and 6750 ps at room temperature – see legend for details. Central part – time-absorption profiles of the spectra shown above at 470, 715, and 1010 nm monitoring the charge separation and charge recombination. Lower part – time-absorption profiles of the spectra in anisole at 470, 715, and 1010 nm monitoring the charge separation and charge recombination

In chlorobenzene, charge separation tends to be faster with 37 ps for  $C_{60}$ -pyr-ZnP, 1 ps for  $C_{60}$ -PPV1-pyr-ZnP and 15 ps for  $C_{60}$ -PPV3-pyr-ZnP, respectively.<sup>57</sup> The radical ion pair states are metastable in all cases and decay on the picosecond/nanosecond time scale. Lifetimes of 1189, 1585, and 320 ps in anisole and 991, 1076, and 250 ps in chlorobenzene for  $C_{60}$ -pyr-ZnP,  $C_{60}$ -PPV1-pyr-ZnP, and  $C_{60}$ -PPV3-pyr-ZnP were determined, respectively (Table 2).<sup>58</sup>

## ARTICLE

**Table 2.** Electron donor–acceptor center-to-center distances, charge separation and charge recombination dynamics, reorganization energies, electronic couplings, and damping factors.

Compound	$R_{DA} / \text{\AA}$	$k_{CS} / s^{-1}$		$k_{CR} / s^{-1}$		$\lambda / eV$	$V / cm^{-1}$	$\beta / \text{\AA}^{-1}$	
		anisole	chlorobenzene	anisole	chlorobenzene			anisole	chlorobenzene
<b>C<sub>60</sub>-pyr•ZnP</b>	10.6	$4 \times 10^{10}$	$2.7 \times 10^{10}$	$8.4 \times 10^8$	$1.0 \times 10^9$	0.78	10	0.24	0.15
<b>C<sub>60</sub>-PPV1-pyr•ZnP</b>	16.8	$5 \times 10^{11}$	$1 \times 10^{12}$	$6.3 \times 10^8$	$9.3 \times 10^8$	0.74	57		
<b>C<sub>60</sub>-PPV3-pyr•ZnP</b>	30.0	$4.3 \times 10^{10}$	$6.7 \times 10^{10}$	$3.1 \times 10^9$	$4.0 \times 10^{10}$	0.91	35		
		THF	benzonitrile	THF	benzonitrile			benzonitrile	
<b>C<sub>60</sub>-oPPV3-ZnP</b>	25.0	$4.5 \times 10^{9*}$	$3.2 \times 10^{9*}$	$1.2 \times 10^{6*}$	$4.4 \times 10^{6*}$	0.72	4.9*	0.03*	
<b>C<sub>60</sub>-oPPV5-ZnP</b>	39.0	$3.2 \times 10^{9*}$	$4.4 \times 10^{9*}$	$9.3 \times 10^{5*}$	$2.7 \times 10^{6*}$	0.72	4.1*		

\*G. de la Torre, F. Giacalone, J. L. Segura, N. Martín and D. M. Guldi, *Chem. -Eur. J.*, 2005, **11**, 1267-1280.

## ARTICLE

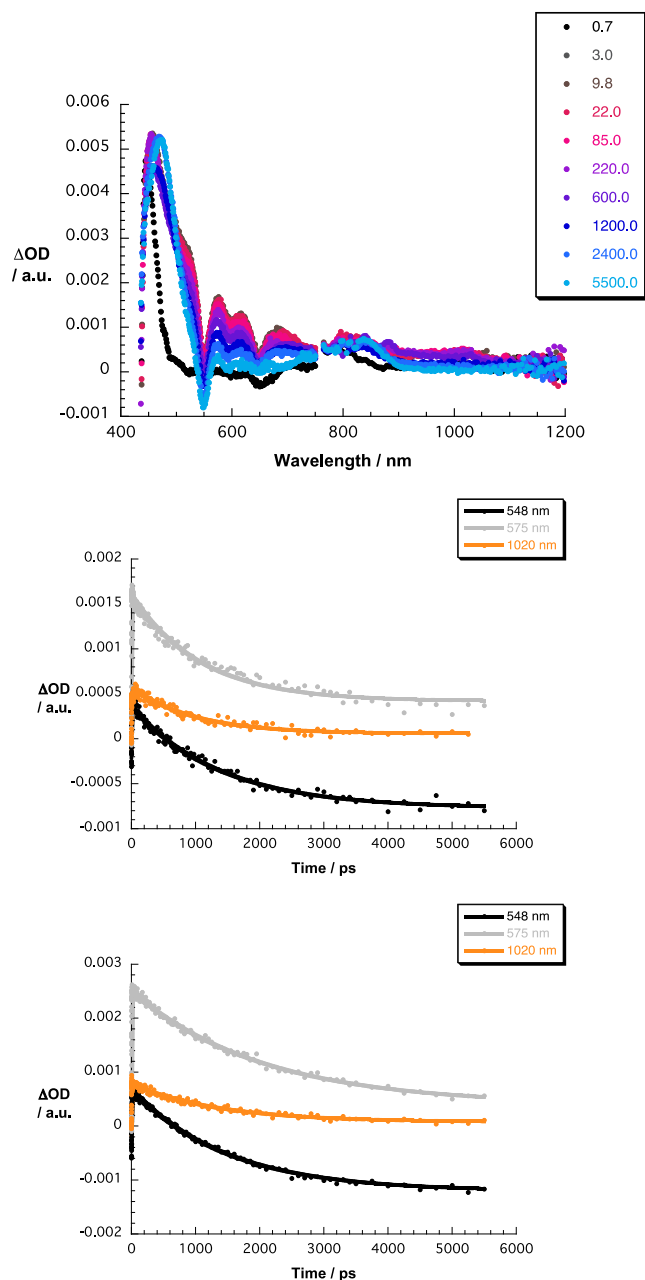


**Fig. 5.** Upper part – differential absorption spectra (visible) obtained upon pump probe excitation (420 nm, 200 nJ) of  $C_{60}$ -pyr•ZnP (in a 1 to 5 ratio) in chlorobenzene with several time delays between 0.7 and 5500 ps at room temperature – see legend for details. Central part – time-absorption profiles of the spectra shown above at 548, 575, and 1020 nm monitoring the charge separation and charge recombination. Lower part – time-absorption profiles of the spectra in anisole at 548, 575, and 1020 nm monitoring the charge separation and charge recombination.

The fact that charge recombination in  $C_{60}$ -PPV3-pyr•ZnP is faster than in  $C_{60}$ -pyr•ZnP and  $C_{60}$ -PPV1-pyr•ZnP despite the larger electron donor-acceptor separations is surprising. At first glance, it may be rationalized by invoking different total reorganization energies of the electron donor-acceptor ensembles due to larger electron donor-acceptor separations. To determine the reorganization energies for  $C_{60}$ -pyr•ZnP,  $C_{60}$ -PPV1-pyr•ZnP, and  $C_{60}$ -PPV3-pyr•ZnP, the energy levels of the corresponding radical ion pair states were estimated using the continuum model for electron transfer (Equation 1),<sup>59</sup>

$$E_{IP} = E_{ox} - E_{red} - \frac{1}{4\pi\epsilon_0} \frac{e^2}{\epsilon_s R_{DA}} + \frac{e^2}{4\pi\epsilon_0} \left( \frac{1}{2r_D} + \frac{1}{2r_A} \right) \left( \frac{1}{\epsilon_s} - \frac{1}{\epsilon'_s} \right) \quad (1)$$

where  $E_{ox}$  and  $E_{red}$  are the oxidation and reduction potentials, respectively,  $e$  is the electronic charge,  $\epsilon_0$  is the dielectric constant of vacuum,  $\epsilon_s$  is the static dielectric constant of the solvent, in which the rate constants are measured,  $\epsilon'_s$  is the dielectric constant of the solvent, in which  $E_{ox}$  and  $E_{red}$  are measured,  $R_{DA}$  is the electron donor-acceptor center-to-center distance, and  $r_D$  and  $r_A$  are the spherical radii of the electron donor and acceptor, respectively. Notably, the  $R_{DA}$  are 10.6, 16.8, and 30 Å for  $C_{60}$ -pyr•ZnP,  $C_{60}$ -PPV1-pyr•ZnP, and  $C_{60}$ -PPV3-pyr•ZnP. The spherical radii of the electron donor and acceptor are  $r_D = 5.0$  Å and  $r_A = 4.4$  Å, respectively.  $E_{ox} - E_{red}$  is 1.52, 1.57 and 1.57 V for  $C_{60}$ -pyr•ZnP,  $C_{60}$ -PPV1-pyr•ZnP, and  $C_{60}$ -PPV3-pyr•ZnP, respectively.

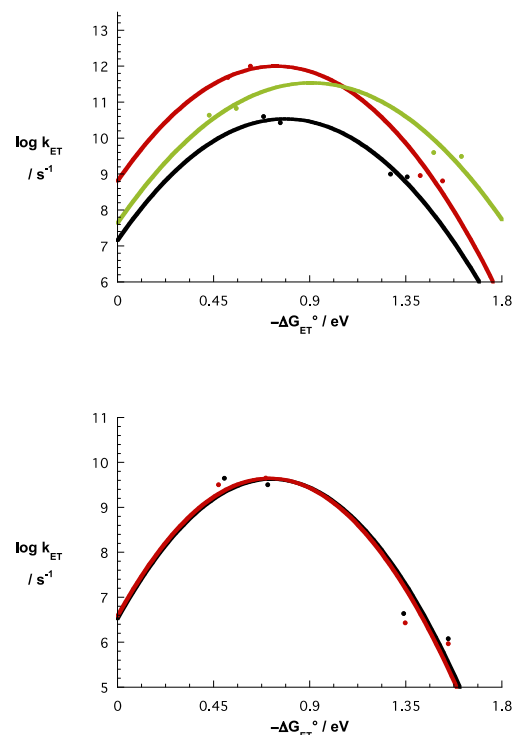


**Fig. 6.** Upper part – driving force ( $-\Delta G_{ET}^0$ ) dependences of the rate constants for charge separation and charge recombination for  $C_{60}$ -PPV1-pyr•ZnP (red),  $C_{60}$ -PPV3-pyr•ZnP (green), and  $C_{60}$ -pyr•ZnP (black). Lower part – driving force ( $-\Delta G_{ET}^0$ ) dependences of the rate constants for

charge separation and charge recombination for  $C_{60}$ -oPPV<sub>3</sub>-ZnP (black) and  $C_{60}$ -oPPV<sub>5</sub>-ZnP (red).

$$k_{ET} = \sqrt{\frac{\rho}{\hbar/k_B T}} |V|^2 \exp\left(-\frac{(DG_{ET}^0 + \lambda)^2}{4/k_B T}\right) \quad (2)$$

The driving forces for charge-separation were evaluated by relating the aforementioned energy levels to those of the excited-state precursors, while those for the charge-recombination were taken from the radical ion pair states. Next, the electron transfer rate constants ( $k_{ET}$ ), that is, charge-separation and charge-recombination, were treated as a function of driving forces ( $-\Delta G_{ET}^0$ ), within the framework of the classical Marcus theory – equation 2.<sup>30</sup> In equation 2,  $k_B$  is the Boltzmann constant,  $V$  is the electronic coupling, and  $\lambda$  is the reorganization energy. The classical Marcus theory helps in shedding light onto the total reorganization energies  $\lambda$  (Figure 6).

The fits of the Marcus parabola give a total reorganization energy of 0.91 eV for  $C_{60}$ -PPV3-pyr-ZnP, substantially larger than that derived for  $C_{60}$ -PPV1-pyr-ZnP (0.74 eV).  $C_{60}$ -pyr-ZnP is an interesting case because its reorganization energy of 0.78 eV is larger than that of  $C_{60}$ -PPV1-pyr-ZnP but smaller than that of  $C_{60}$ -PPV3-pyr-ZnP. A likely reason involves enhanced ground-state interactions in  $C_{60}$ -pyr-ZnP leading to electronic perturbation and, in turn, to a larger total reorganization energy.<sup>7</sup> Implicit are rather large contributions from the internal reorganization energies as particularly evident in  $C_{60}$ -pyr-ZnP. Considering electron donor-acceptor distances of 10.6, 16.8, 30 Å in the non-covalent assemblies, we can also draw conclusions about the reorganization energies for  $C_{60}$ -ZnP conjugates, in which the electron donor and the electron acceptor are covalently linked rather than non-covalently assembled (Figure 6). To this end, we determined distance-independent values for  $C_{60}$ -oPPV-ZnPs of 0.72 eV with oPPV trimers and pentamers, which correspond to electron donor-acceptor distances of 25 and 39 Å, respectively.<sup>18</sup>

Interesting is the fact that the electronic couplings are 57, 35, and 10  $cm^{-1}$  for  $C_{60}$ -PPV1-pyr-ZnP,  $C_{60}$ -PPV3-pyr-ZnP, and  $C_{60}$ -pyr-ZnP, respectively. The difference between the latter one and the earlier two might be rationalized on the basis of different electron transfer mechanisms, that is, through space versus through bond.

To dissect the impact of the non-covalent assembly on the electron-transfer features we turned to the distance dependence of electron transfer by analyzing the charge separation in anisole and chlorobenzene. The damping factor  $\beta$  was estimated by means of equation 3, where,  $k_0$  is the preexponential factor,  $\beta$  is the damping factor, and  $R_{DA}$  is the electron donor-acceptor distance.

$$k_{ET} = k_0 \exp(-\beta R_{DA}) \quad (3)$$

At first glance, and in stark contrast to the low damping factors found for  $C_{60}$ -oPPV-ZnPs with values as low as 0.03 Å<sup>-1</sup>,<sup>18</sup> in  $C_{60}$ -oPPV-ZnPs the value is 0.08 Å<sup>-1</sup> when plotting the maximum rate constant (Figure 7). The sole difference between  $C_{60}$ -oPPV-ZnPs and  $C_{60}$ -oPPV-ZnPs is the linkage, that is, either covalently via the peripheral phenyl groups or non-covalently via the central zinc. A closer look at the local electron affinity maps for  $C_{60}$ -pyr-ZnP,  $C_{60}$ -PPV1-pyr-ZnP, and  $C_{60}$ -PPV3-pyr-ZnP versus  $C_{60}$ -oPPV3-ZnP and  $C_{60}$ -oPPV5-ZnP corroborates a fairly homogeneous pathway for electrons from the photoexcited/electron donating ZnP to the electron accepting  $C_{60}$  in the latter. In the earlier, the same homogeneity prevails but comes to a sudden stop at the pyridinic nitrogen. In other words, the nitrogen emerges as a bottleneck in the electron transport through  $C_{60}$ -pyr-ZnP,  $C_{60}$ -PPV1-pyr-ZnP, and  $C_{60}$ -PPV3-pyr-ZnP and, in turn, increases the damping factor.

A final consideration is associated with the local electronic affinity maps, which clearly reveal distributions of low local electron affinity at the zinc spilling over to the pyridinic nitrogen for the coordinative compounds (Figure 8). As a matter of fact, a delocalization of the ZnP radical cation throughout the porphyrin including the central zinc assists in rationalizing the fairly large

reorganization energies in  $C_{60}$ -pyr-ZnP,  $C_{60}$ -PPV1-pyr-ZnP, and  $C_{60}$ -PPV3-pyr-ZnP and, more importantly, its distance dependence.

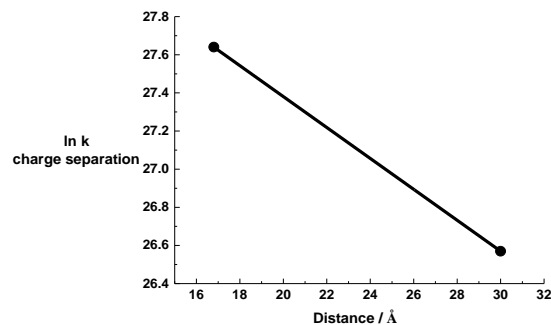


**Fig. 7.** Distance dependence of electron-transfer rate constants in  $C_{60}$ -PPV1-pyr-ZnP and  $C_{60}$ -PPV3-pyr-ZnP in nitrogen-saturated anisole (black) and chlorobenzene (red) at room temperature.

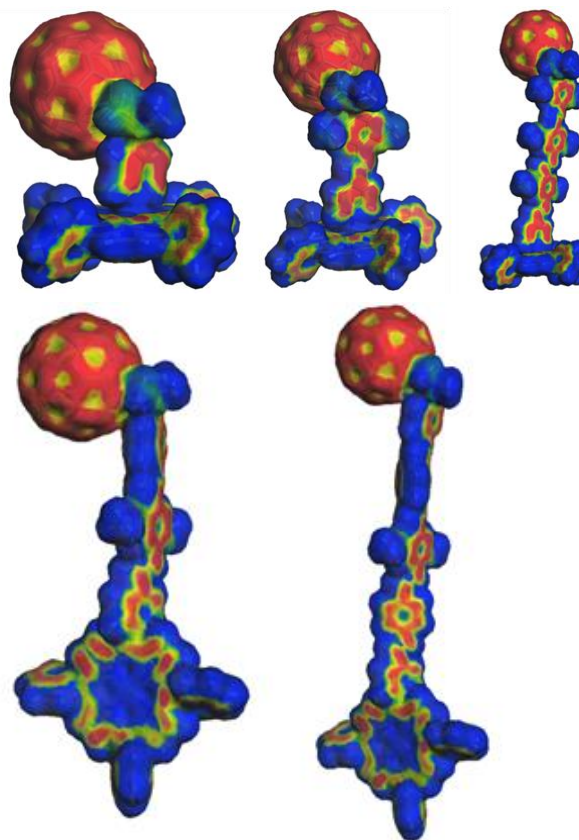


**Fig. 8.** Upper part - EA<sub>L</sub> mapped from -80.0 (blue) to -30.0 kcal mol<sup>-1</sup> (red) onto the electronic density isosurfaces (0.03 e<sup>-</sup> Å<sup>-3</sup>) of  $C_{60}$ -pyr-ZnP,  $C_{60}$ -PPV1-pyr-ZnP, and  $C_{60}$ -PPV3-pyr-ZnP. Lower part) EA<sub>L</sub> mapped from -80.0 (blue) to -30.0 kcal mol<sup>-1</sup> (red) onto the electronic density isosurfaces (0.03 e<sup>-</sup> Å<sup>-3</sup>) of  $C_{60}$ -oPPV<sub>3</sub>-ZnP and  $C_{60}$ -oPPV<sub>5</sub>-ZnP.

In addition, the lowest-lying singlet charge-transfer state of  $C_{60}$ -pyr-ZnP shows significant deviations from the ground state geometry as it moves the charged moieties closer together. The axial Zn-N bond is bent approximately 2° towards the electron accepting  $C_{60}$  and the pyridine ring assumes a distinct boat conformation with 9° and 5° deviations from planarity (Figure 9). These distortions result in the charged  $C_{60}$  moving approximately 1 Å closer to one of

the twisted phenyl substituents, allowing stabilization by CH...C hydrogen bonding. The latter turns out to be quite favorable in this case because of the negative charge on C<sub>60</sub>. The charge-transfer nature of this state is demonstrated unambiguously by the calculated (AM1-CI) molecular electrostatic potential on the 0.001 a.u. isodensity surface. It corresponds approximately to the van der Waals surface shown in Figure 9. Regarding C<sub>60</sub>-PPV1-pyr•ZnP and C<sub>60</sub>-PPV3-pyr•ZnP no particular CT states were calculable due to the rather large distances between electron donors and acceptors.

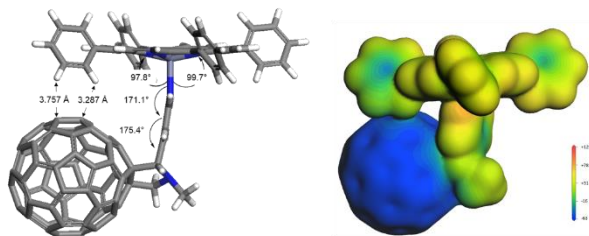


**Fig. 9.** Left part – geometry of the lowest-lying singlet charge-transfer state of C<sub>60</sub>-pyr•ZnP. Right part – electrostatic potential on the 0.001 a.u. isodensity surface calculated by AM1-CI.

## Conclusions

The integration of ZnP into short and long oPPVs bearing C<sub>60</sub>, namely C<sub>60</sub>-PPV1-pyr and C<sub>60</sub>-PPV3-pyr is accomplished via coordination to pyridyl groups. As such, the corresponding C<sub>60</sub>-PPV1-pyr•ZnP and C<sub>60</sub>-PPV3-pyr•ZnP are fully characterized by complementary spectroscopic means, but fail to give rise to appreciable electronic interactions in the ground state. In the excited state, electronic interactions between photoactive ZnP and C<sub>60</sub>-PPV1-pyr and C<sub>60</sub>-PPV3-pyr are inferred from fluorescence spectroscopy. By means of transient absorption measurements we confirmed that the excited state interactions leads to the formation of radical ion pair states, that is, the one electron oxidized ZnP radical cation and the one electron reduced C<sub>60</sub> radical anion. In both instances the radical ion pair states are metastable with, however, C<sub>60</sub>-PPV3-pyr•ZnP showing a faster charge recombination than C<sub>60</sub>-PPV1-pyr•ZnP despite the larger electron donor-acceptor separation. This rather surprising result stems from a distinct distance dependence found for C<sub>60</sub>-PPV1-pyr•ZnP and C<sub>60</sub>-PPV3-pyr•ZnP with electron donor-acceptor distances of 16.8 and 30 Å and with reorganization energies of 0.74 and 0.91 eV, respectively. On the contrary, linking ZnP covalently to C<sub>60</sub>-oPPVs at, for example, electron donor-acceptor distances between 24.9 and 38.7 Å leads to invariant reorganization energies of around 0.72 eV. This difference goes hand in hand with changes in the damping factor with values as low as 0.03 Å<sup>-1</sup> for the covalently linked conjugates and as high as 0.08 Å<sup>-1</sup> for C<sub>60</sub>-PPV1-pyr•ZnP and C<sub>60</sub>-PPV3-pyr•ZnP. Insights into the noted differences came from molecular modeling, which disclosed that the fairly homogeneous pathway for electrons from the electron-donating ZnP to the electron-accepting C<sub>60</sub> is suddenly disrupted at the pyridinic nitrogen. In light of the aforementioned, the ability to control electron transfer rates by modulating the reorganization energy in non-covalent ensembles opens new perspectives for the design and preparation of new architectures potentially efficient for energy applications.

## Acknowledgements

Financial support from the European Commission (FP7-REGPOT-2008-1, Project BIOSOLENUTI No 229927) is greatly acknowledged. This research has been also co-financed by the European Union (European Social Fund – ESF) and Greek national funds through the Operational

Program "Education and Lifelong Learning" of the National Strategic Reference Framework (NSRF)-Research Funding Program: Heraklitos II. Finally Special Research account of the University of Crete is also acknowledged. Partial financial support by the Greek General Secretariat for Research and Technology and the European Commission, through the European Fund for Regional Development, NSRF 2007-2013 action "Development of Research Centers – ΚΡΗΤΙΣ", project 447963 "New Multifunctional Nanostructured Materials and Devices – POLYNANO" to NT is acknowledged. This work has been supported by MICINN and MEC, Spain (CTQ-2011-24187/BQU and PIB2010US-00652). J. T. Margraf is supported by a Beilstein Foundation scholarship. S. Kuhri and C. Schubert are supported by EAM, and C. Stangel by Heraklitos II.

## Notes and references

<sup>1</sup>Department of Chemistry, University of Crete, Laboratory of Bioinorganic Chemistry, Voutes Campus, P.O. Box 2208, 71003 Heraklion, Crete, Greece, E-mail: [coutsole@chemistry.uoc.gr](mailto:coutsole@chemistry.uoc.gr)

<sup>2</sup>Theoretical and Physical Chemistry Institute, National Hellenic Research Foundation,

48 Vassileos Constantinou Avenue, Athens 11635, Greece, E-mail: [tagmatar@cie.gr](mailto:tagmatar@cie.gr)

<sup>3</sup>Department of Chemistry and Pharmacy, Interdisciplinary Center for Molecular Materials (ICMM), Friedrich-Alexander-Universität Erlangen-Nuernberg, Egerlandstr. 3, 91058 Erlangen, Germany, E-mail: [dirk.guldi@fau.de](mailto:dirk.guldi@fau.de)

<sup>4</sup>Computer Chemie Centrum, Department of Chemistry and Pharmacy, Friedrich-Alexander-Universität Erlangen-Nuernberg, Naegelsbachstraße 25, 91052 Erlangen, Germany, Email: [tim.clark@fau.de](mailto:tim.clark@fau.de)

<sup>5</sup>Institute of Chemistry, University of Białystok, Hurtowa 1, 15-399 Białystok, Poland.

<sup>6</sup>Departamento de Química Organica, Universidad Autonoma de Madrid, Cantoblanco, 28049-Madrid Spain.

<sup>7</sup>IMDEA-Nanociencia, C/Faraday, 9, Cantoblanco, 28049-Madrid, Spain

### Author Contributions

<sup>#</sup>These authors contributed equally to this work

† Footnotes should appear here. These might include comments relevant to but not central to the matter under discussion, limited experimental and spectral data, and crystallographic data.

Electronic Supplementary Information (ESI) available: [details of any supplementary information available should be included here]. See DOI: 10.1039/b000000x/

1. M. R. Wasielewski, *Chem. Rev.*, 1992, **92**, 435-461.
2. R. E. Blankenship, *Molecular Mechanisms of Photosynthesis*, Blackwell Science, Oxford, U.K., 2002.
3. D. Gust, T. A. Moore and A. L. Moore, *Acc. Chem. Res.*, 1993, **26**, 198-205.
4. H. B. Gray and J. R. Winkler, *Annu. Rev. Biochem.*, 1996, **65**, 537-561.
5. M. Grätzel, *Journal of Photochemistry and Photobiology C: Photochemistry Reviews*, 2003, **4**, 145-153.
6. T. Nakanishi, *Supramolecular Soft Matter, Applications in Materials and Organic Electronics*, John Wiley & Sons: , New Jersey., 2011.
7. D. M. Guldi, *Chem. Soc. Rev.*, 2002, **31**, 22-36.
8. F. D'Souza, *Handbook of Carbon Nanomaterials, Synthesis and Supramolecular Systems*, World Scientific Publishing Co. Pte. Ltd, Singapore, 2011.

9. H. Imahori, Y. Mori and Y. Matano, *Journal of Photochemistry and Photobiology C-Photochemistry Reviews*, 2003, **4**, 51-83.
10. V. Balzani, A. Credi and M. Venturi, *ChemSusChem*, 2008, **1**, 26-58.
11. M. E. El-Khouly, O. Ito, P. M. Smith and F. D'Souza, *Journal of Photochemistry and Photobiology C: Photochemistry Reviews*, 2004, **5**, 79-104.
12. Kadish K., Smith K.M. and Guillard R., *The porphyrin handbook* Academic Press., San Diego, London, 2000.
13. H. Imahori, H. Yamada, D. M. Guldi, Y. Endo, A. Shimomura, S. Kundu, K. Yamada, T. Okada, Y. Sakata and S. Fukuzumi, *Angew. Chem. Int. Ed.*, 2002, **41**, 2344-2347.
14. S. Fukuzumi, K. Ohkubo, H. Imahori and D. M. Guldi, *Chem. - Eur. J.*, 2003, **9**, 1585-1593.
15. J.-F. N. F. Langa, *Fullerenes: Principles and Applications, Nanoscience and Nanotechnology Series*, The Royal Society of Chemistry, Cambridge, U.K, 2007.
16. N. M. D. M. Guldi, *Fullerenes: From Synthesis to Optoelectronic Applications*, Kluwer Academic, Dordrecht, 2002.
17. F. Giacalone, J. L. Segura, N. Martín, J. Ramey and D. M. Guldi, *Chem. -Eur. J.*, 2005, **11**, 4819-4834.
18. G. de la Torre, F. Giacalone, J. L. Segura, N. Martín and D. M. Guldi, *Chem. -Eur. J.*, 2005, **11**, 1267-1280.
19. G. Accorsi, N. Armaroli, J.-F. Eckert and J.-F. Nierengarten, *Tetrahedron Lett.*, 2002, **43**, 65-68.
20. J. L. Segura, R. Gomez, N. Martin, C. Luo, A. Swartz and D. M. Guldi, *Chem. Commun.*, 2001, 707-708.
21. D. M. Guldi, A. Swartz, C. Luo, R. Gómez, J. L. Segura and N. Martín, *J. Am. Chem. Soc.*, 2002, **124**, 10875-10886.
22. F. Langa, M. a. J. Gómez-Escalonilla, E. Díez-Barra, J. n. C. García-Martínez, A. de la Hoz, J. Rodríguez-López, A. González-Cortés and V. López-Arza, *Tetrahedron Lett.*, 2001, **42**, 3435-3438.
23. J.-F. Nierengarten, N. Armaroli, G. Accorsi, Y. Rio and J.-F. Eckert, *Chem. -Eur. J.*, 2003, **9**, 36-41.
24. T. Nhu Y Hoang, D. Pocięcha, M. Salamoczyk, E. Gorecka and R. Deschenaux, *Soft Matter*, 2011, **7**, 4948-4953.
25. T. M. Figueira-Duarte, Y. Rio, A. Listorti, B. Delavaux-Nicot, M. Holler, F. Marchioni, P. Ceroni, N. Armaroli and J.-F. Nierengarten, *New J. Chem.*, 2008, **32**, 54-64.
26. J. Santos, B. M. Illescas, M. Wielopolski, A. M. G. Silva, A. C. Tomé, D. M. Guldi and N. Martín, *Tetrahedron*, 2008, **64**, 11404-11408.
27. F. Giacalone, J. L. Segura, N. Martín and D. M. Guldi, *J. Am. Chem. Soc.*, 2004, **126**, 5340-5341.
28. D. M. Guldi, B. M. Illescas, C. M. Atienza, M. Wielopolski and N. Martin, *Chem. Soc. Rev.*, 2009, **38**, 1587-1597.
29. N. Armaroli, F. Barigelletti, P. Ceroni, J.-F. Eckert, J.-F. Nicoud and J.-F. Nierengarten, *Chem. Commun.*, 2000, 599-600.
30. R. A. Marcus, *J. Chem. Phys.*, 1956, **24**, 966-978.
31. R. A. Marcus, *J. Chem. Phys.*, 1965, **43**, 679-701.
32. E. Peeters, P. A. van Hal, J. Knol, C. J. Brabec, N. S. Sariciftci, J. C. Hummelen and R. A. J. Janssen, *J. Phys. Chem. B*, 2000, **104**, 10174-10190.
33. J.-F. Eckert, J.-F. Nicoud, J.-F. Nierengarten, S.-G. Liu, L. Echegoyen, F. Barigelletti, N. Armaroli, L. Ouali, V. Krasnikov and G. Hadziioannou, *J. Am. Chem. Soc.*, 2000, **122**, 7467-7479.
34. N. Armaroli, G. Accorsi, J.-P. Gisselbrecht, M. Gross, V. Krasnikov, D. Tsamouras, G. Hadziioannou, M. J. Gomez-Escalonilla, F. Langa, J.-F. Eckert and J.-F. Nierengarten, *J. Mater. Chem.*, 2002, **12**, 2077-2087.
35. A. M. Ramos, S. C. J. Meskers, P. A. van Hal, J. Knol, J. C. Hummelen and R. A. J. Janssen, *J. Phys. Chem. A*, 2003, **107**, 9269-9283.
36. A. Gégout, J.-F. Nierengarten, B. Delavaux-Nicot, C. Duhayon, A. Saquet, A. Listorti, A. Belbakra, C. Chiorboli and N. Armaroli, *Chem. -Eur. J.*, 2009, **15**, 8825-8833.
37. A. Gégout, J. L. Delgado, J.-F. Nierengarten, B. Delavaux-Nicot, A. Listorti, C. Chiorboli, A. Belbakra and N. Armaroli, *New J. Chem.*, 2009, **33**, 2174-2182.
38. D. M. Guldi and V. Sgobba, *Chem. Commun.*, 2011, **47**, 606-610.
39. T. Hasobe, *Phys. Chem. Chem. Phys.*, 2012, **14**, 15975-15987.
40. T. Umeyama and H. Imahori, *J. Phys. Chem. C*, 2012, **117**, 3195-3209.
41. J.-M. Lehn, *P. Natl. Acad. Sci.*, 2002, **99**, 4763-4768.
42. J. F. Stoddart and H.-R. Tseng, *P. Natl. Acad. Sci.*, 2002, **99**, 4797-4800.
43. C. C. Armarego W. L. F., *Purification of Laboratory Chemicals*, 6th edn., Elsevier Inc, Oxford, 2009.
44. P. Rothmund and A. R. Menotti, *J. Am. Chem. Soc.*, 1948, **70**, 1808-1812.
45. B. Ehresmann, B. Martin, A. H. C. Horn and T. Clark, *J. Mol. Model.*, 2003.
46. M. J. S. Dewar, E. G. Zebisch, E. F. Healy and J. J. P. Stewart, *J. Am. Chem. Soc.*, 1985, **107**, 3902-3909.
47. T. T. Clark and M. Hennemann, EMPIRE'12, 2011.
48. B. Ehresmann, B. Martin, A. C. Horn and T. Clark, *J. Mol. Model.*, 2003, **9**, 342-347.
49. T. Clark, *J. Mol. Model.*, 2010, **16**, 1231-1238.
50. M. Prato and M. Maggini, *Acc. Chem. Res.*, 1998, **31**, 519-526.
51. J. Boutagy and R. Thomas, *Chem. Rev.*, 1974, **74**, 87-99.
52. P. Shao, Z. Li, J. Luo, H. Wang and J. Qin, *Synth. Commun.*, 2005, **35**, 49-53.
53. B. Wang and M. R. Wasielewski, *J. Am. Chem. Soc.*, 1997, **119**, 12-21.
54. D. M. Guldi and M. Prato, *Acc. Chem. Res.*, 2000, **33**, 695-703.
55. V. A. Walters, J. C. de Paula, B. Jackson, C. Nutaitis, K. Hall, J. Lind, K. Cardozo, K. Chandran, D. Raible and C. M. Phillips, *J. Phys. Chem.*, 1995, **99**, 1166-1171.
56. J. Fajer, D. C. Borg, A. Forman, D. Dolphin and R. H. Felton, *J. Am. Chem. Soc.*, 1970, **92**, 3451-3459.
57. In addition, we note a second, slower electron transfer process in C<sub>60</sub>-PPV1-pyr•ZnP, which evolves from C<sub>60</sub> singlet excited state generated by means of an initial excited state energy transfer.
58. Importantly, the charge recombination reinstates the ground state rather than the triplet excited state of, for example, the ZnP. This pathway was confirmed in singlet oxygen measurements as a reflection of the ZnP and C<sub>60</sub> triplet excited state quantum yields. In titration experiments, where an excess of ZnP (10:1 and 30:1)

was present, a C<sub>60</sub> concentration dependent and gradual decrease of the singlet oxygen emission was noted.

59. A. Weller, *Z. Phys. Chem. Neue Folge*, 1982, **133**, 93-98.